Fingerprinting subduction margins using PCA profiles: A data science approach to assessing earthquake hazard

Valerie Locher[1], Rebecca E. Bell[1], Parastoo Salah[1], Robert Platt[1], Cédric M. John[2,1]

[1]*Imperial College London, Department of Earth Science and Engineering, Royal School of Mines, London, SW7 2AZ, United Kingdom*

[2]*now at: Queen Mary University of London, Digital Environment Research Institute, Empire House, 67-75 New Road, London, E1 1HH, United Kingdom*

ABSTRACT

Giant earthquakes ($M_W \geq 8.5$) along subduction margins pose great hazards to coastal societies. While it is generally accepted that geological margin properties play a role, the controls on giant earthquake occurrence remain undetermined. Their long intermittence times and the comparatively short earthquake record obscure any correlations between margin properties and seismicity.

This work presents a new approach to relating margin properties to seismicity. We apply Principal Component Analysis (PCA) to a set of margin properties to "fingerprint" margins by assigning them a PCA profile, which we compare to giant earthquake occurrence . This approach reduces bias from the short earthquake record as seismicity is not used as a PCA input feature. Using Kernel-PCA, a non-linear PCA variant, we uncover non-linear patterns in margin properties, and suggest that links between these properties and seismicity are non-linear., which helps explain why they have previously been hard to establish.

PCA clusters identify "active and moderate" and "quiet and extreme" margins (following Ide, 2013). We argue that margin segments with "quiet and extreme" PCA profiles, but no giant earthquakes since 1900, should be considered as hazardous as those that have ruptured in giant earthquakes recently.

Corresponding author: *Valerie Locher, valerie.locher22@imperial.ac.uk*

This is a non-peer reviewed preprint submitted to EarthArXiv. Subsequent versions of this manuscript may have slightly different content. This preprint has been submitted for peer review to Geology. This version of the manuscript has been modified to incorporate one round of feedback from three peer reviewers.

INTRODUCTION

Giant earthquakes ($M_W \geq 8.5$) along subduction margins, such as the 2004 Sumatra-Andaman, 2010 Chile, and 2011 Tohoku earthquakes pose serious hazards to coastal societies. The mechanisms that control where giant earthquakes initiate remain uncertain, in part due to their long recurrence times. Not all subduction margins have experienced giant earthquakes since 1900, the start of our well-documented seismic record (e.g. McCaffrey, 2008; Schellart & Rawlinson, 2013). This poses the question whether certain geological margin properties enable or inhibit large earthquakes (e.g. Ruff, 1989). Alternatively, perhaps all subduction margins can initiate large earthquakes and the apparent lack thereof is simply down to the short earthquake record (e.g. Stein & Okal, 2007; McCaffrey, 2008).

The geological controls on subduction margin seismicity have been explored in some detail in recent years, both focusing on single margins (e.g. McCaffrey, 2009; Wallace et al., 2009) and considering global data compilations of margin properties (e.g. Ruff, 1989; Schellart & Rawlinson, 2013). Early interpretations linked giant earthquake occurrence to fast-converging young plates, as opposed to slower-converging older plates, suggesting that plate density and convergence rate control seismicity (e.g. Ruff & Kanamori, 1980). However, this model could not explain the 2004 Sumatra and 2011 Tohoku earthquakes, which occurred in areas of slow convergence and old plate age respectively (Stein & Okal, 2007, 2011). Further studies explored other properties such as the seabed roughness of the incoming plate, which has been linked to intraplate coupling (e.g. Lallemand et al., 2018) or its bending angle, thought to influence seismogenic zone width and plate hydration (e.g. Nishikawa & Ide, 2015). Multiple studies noted correlations between locations of high sediment thickness and giant earthquakes, concluding that abundant sediment availability increases intraplate locking (e.g. Ruff, 1989; Heuret et al., 2012; Scholl et al., 2015).

However, the 1952 Kamchatka and 2011 Tohoku earthquakes (both M_W 9) challenge this hypothesis as they occurred in areas of fairly low sediment thickness (Scholl et al., 2015).

Based on these observations, and the variety of processes occurring at subduction margins, many have concluded that subduction margin seismicity is determined by a complex interplay of multiple factors (e.g. Wallace et al., 2009; Schellart & Rawlinson, 2013; Wirth et al., 2022). Recent studies thus examined connections between margin properties and maximum observed earthquake magnitude using multivariate statistics and regression approaches (e.g. Brizzi et al., 2018; Nakao et al., 2023). However, short measurement and historical records compared to giant earthquake intermittence times often lead to underestimated maximum magnitudes, meaning such models are trained on incomplete data.

We present an unsupervised data science approach to exploring correlations between four margin properties (sediment thickness, relative plate velocity, and the subducting plate's dip angle and roughness) and maximum magnitude. We fingerprint margin segments by applying linear and Kernel-Principal Component Analyses (PCA) to project the property data into a lower dimensional orthogonal vector space where their location is described by their PCA profile. By excluding the maximum observed magnitude data from the PCA input and using it only to infer the seismic behaviour of different PCA profiles, we reduce bias resulting from the short earthquake record. We observe correlations between PCA profiles and maximum magnitude which we apply to assess the possibility of giant earthquake occurrence for margins with no giant earthquakes since 1900. Our results suggest that connections between margin properties and seismic behaviour are non-linear.

METHODS

Data Preprocessing

We utilize a dataset that encompasses sediment thickness, dip angle, roughness, and relative velocity for 1540 25x200km margin segments, oriented with their long axis orthogonally to and centred on the subduction trench along margins (compiled by McLellan & Audet, 2020 for a study investigating the relationship between margin properties and slow slip). Roughness values were derived from gravimetry data and thus best represent the roughness of the oceanic basement (see Smith (2014); Bassett and Watts (2015) for context on determining roughness). Data pre-processing for these properties included imputing missing values, scaling the data (see Supplemental Material), and log-transforming the roughness, dip, and sediment thickness values.

Considering earthquake data from the U.S. Geological Survey (1900 - 2023) as well as historical earthquakes from the global historical earthquake catalogue (Albini et al., 2013), we assign each segment a maximum observed magnitude (Fig. 1) using a custom binning algorithm: for each earthquake in the catalogue we calculate the length of rupture using the empirical relationships from Wells and Coppersmith (1994) and draw a circle with diameter of the rupture length around the earthquake's epicentre. Any segment lying within this circle is assigned the earthquake's magnitude. We recognise that rupture lengths and geometries are more complicated, but bespoke rupture geometry information is only available for a small number of well characterised events and thus cannot be used in our global study. The supplemental Fig. S9 shows a comparison of surface rupture lengths as estimated here with finite fault rupture models for 63 events.

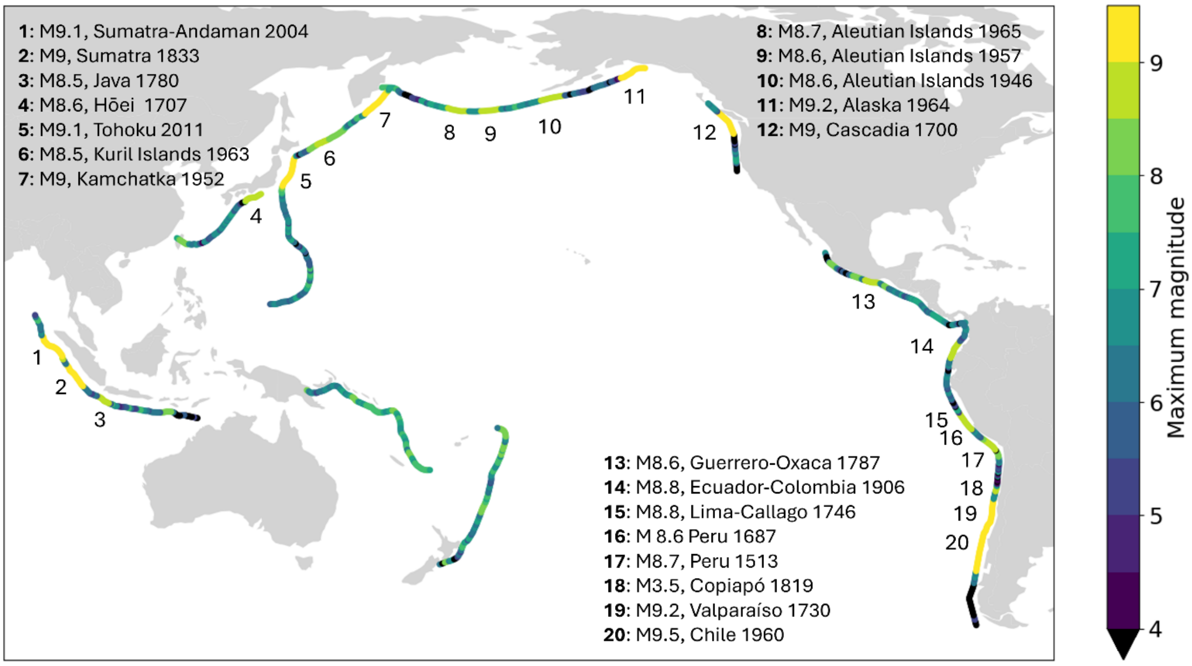

Figure 1: Map showing observed maximum magnitudes for the considered margins.

Principal Component Analysis

Principal Component Analysis (PCA) is a method to reorient data along orthogonal axes of highest variance, known as its principal components (PCs) (Jolliffe, 2002). As PCs are numbered in order of decreasing amount of explained variance in the original data, considering only the first few PCs (e.g. PC1 and PC2 here) can reduce a dataset's dimensionality while retaining most of its information. By applying PCA to margin property data we observe margin segments in an interpretable 2D space while considering multiple properties. Kernel-PCA (Schölkopf et al., 1998) uses kernels to map data to a higher-dimensional space before PCA, whereby different kernels result in different projections. This enables the detection of complex, non-linear patterns that linear methods cannot capture. We generate a diverse set of projections by applying PCA and Kernel-PCA to the margin property data, experimenting with an assortment of kernels, including linear, polynomial, radial basis function (RBF), sigmoid, and cosine. The observed relationships are consistent across PCA types. We here show projections from linear PCA, RBF and cosine Kernel-PCA, which are selected as they capture different non-linear behaviours. This is based on the kernels' differences in calculating the similarity of two points: the RBF kernel estimates the likelihood of two points sharing a Gaussian curve, while the cosine kernel measures similarity based on the angle between vectors (Schölkopf et al., 1998; Liu et al., 2004). The RBF kernel's parameter γ was set to its scikit-learn default value of 1 divided by the number of features. Lower γ values yield projections similar to linear PCA, whereas higher γ obscure the dataset's global structure. For a more detailed explanation of PCA and Kernel-PCA, see the Supplemental Material.

By plotting PC1 against PC2 and mapping the relative density of segments with maximum magnitudes 8.5 and above as contours (see Fig. 3), we infer the possibility of giant earthquake occurrence on any given margin despite having only a partial record of maximum magnitude events. We observe that using a maximum magnitude cutoff of 8 does not change our conclusions (see supplemental Fig. S7).

The code used is available at github.com/gems-val22/subduction_data_analytics. The Supplemental Material contains pair plots and parallel coordinate plots for PCs 1-4 (Fig. S2-6) and Fig. S8 illustrates the percentage of variance explained per PC.

MARGIN FAMILIES IN THE PC SPACE

Fig. 2 shows projections generated with linear PCA, RBF, and cosine Kernel-PCA. We observe that in all projections, segments from the same margin tend to cluster closely in the PC space (Fig. 2ABC), indicating that individual margins have distinct combinations of the properties considered here. These margin clusters appear to form "meta clusters", which we interpret as "margin families" characterized by a similar combination of properties. We calculate 2D Wasserstein distances (Wasserstein, 1969) between each pair of margins to quantify this closeness.

For example, the Cascadia, Hikurangi, and Nankai-Ryukyu clusters belong to the same margin family, as they have similar PCA profiles and low Wasserstein distances (see supplemental Fig. S10-12).This similarity in margin properties is reflected in their seismic behaviour: all three margins show slow slip (e.g. Rogers & Dragert, 2003; Douglas et al., 2005; Nishimura et al., 2013), and historical (pre-1900) and paleo-seismic observations indicate occasional giant earthquake occurrence (Satake et al., 1996; Clark et al., 2019; Fujiwara et al., 2020).

A distinct margin family at high PC1 values includes segments belonging to the Mariana, Solomon, Vanuatu, and Tonga-Kermadec margins (Fig. 2 BC). We note that these margins have oceanic overriding plates and no large island arcs. They have previously been described by Ide (2013) as “active and moderate”, characterised by frequent rupture in moderate-magnitude earthquakes. In contrast, “quiet and extreme” margins (at low PC1 values) show low background seismicity but occasionally rupture in high-magnitude earthquakes (Ide, 2013). This can be seen in Fig. 2 GHI, where the "quiet and extreme" clusters contain most segments with assigned maximum magnitudes ≥ 8.5 (“extreme”) and < 4 (“quiet”). This supports the idea that margins capable of hosting giant earthquakes may experience prolonged quiescence, with the plate boundary locked as strain accumulates.

The observation that the PCA projections delineate the “active and moderate” from the “quiet and extreme” margins suggests that the difference in seismic behaviour is related to a combination of these four properties (sediment thickness, roughness, dip angle, relative plate velocity). Density contour plots (Fig. 2 DEF), show that Kernel-PCA projections separate margin families into individual clusters more effectively than PCA, suggesting this connection is non-linear.

We used Adjusted Rand Index (ARI) scores (Hubert & Arabie, 1985) to quantify how similar the Kernel- and linear PCA projections’ clusters are (ARI = 100% for identical projections). ARI scores of 57.8% (RBF) and 47.0% (cosine) confirm that the Kernel methods capture different behaviours within the margin property dataset than linear PCA. We conclude that while the non-linear methods seem particularly successful in distinguishing between margin families, their consistent grouping across projections underscores the robustness of this fingerprinting approach.

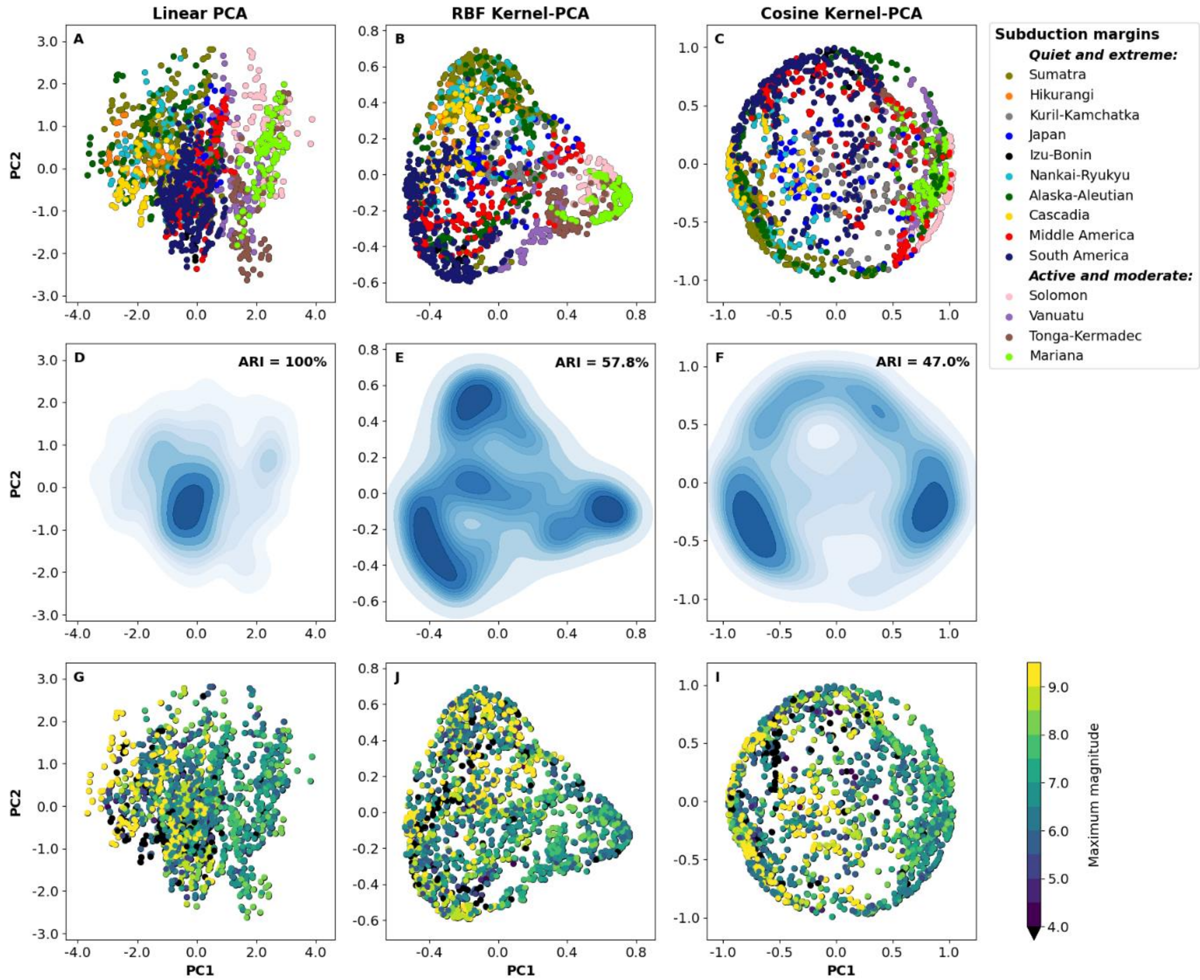

Figure 2: PCA projections generated with linear PCA, RBF and cosine Kernel-PCA. **ABC.** Projected segments by subduction margins; **DEF.** density distribution of segments in the PC space and adjusted rand index scores (ARI; Hubert & Arabie, 1985); **GHI.** projected segments by maximum observed magnitude.

IDENTIFYING MARGINS PRONE TO GIANT EARTHQUAKES

Having established that we can distinguish margin families with different properties and seismicity in the PC space, we utilise the Kernel-PCA projections to assess the possibility of giant earthquake occurrence for margins with potentially underestimated maximum magnitudes. We consider a margin capable of generating giant earthquakes if its PCA profile is similar to high-maximum magnitude ones', indicating similar margin property combinations. Fig. 3 shows the PC space distributions of high-maximum magnitude segments as a density map, to which we compare the PCA profiles of margins with no recorded post-1900 M ≥ 8.5 earthquakes (Hikurangi, Nankai-Ryukyu, Middle America, Solomon, Vanuatu, Mariana, Tonga-Kermadec, Izu-Bonin, Cascadia). Out of these, segments from the Hikurangi, Cascadia, Nankai-Ryukyu, Izu-Bonin, and Middle America margins plot in high-density regions, suggesting they may rupture in giant earthquakes. Historical and paleo-seismic evidence for large earthquakes along the Cascadia (Satake et al., 1996), Hikurangi (Clark et al., 2019) and Nankai-Ryukyu (Fujiwara et al., 2020) trenches supports this assessment.

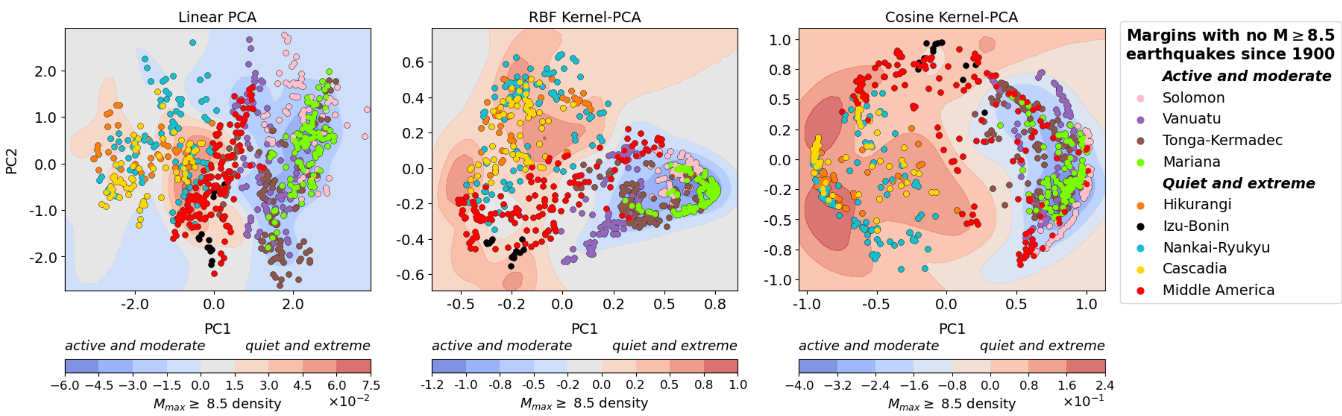

Figure 3: PC space relative density maps of segments with assigned maximum magnitudes of 8.5 and above (filled-in contours) and segment distributions for margins with no giant earthquakes in the instrumental record (scatter points) for projections generated using linear PCA, RBF, and cosine Kernel-PCA.

HOW DO MARGIN PROPERTIES INFLUENCE SEISMICITY?

Fig. 2 and 3 show that a (non-linear) combination of margin properties can distinguish between different seismic behaviours. To examine the individual margin properties' influence on the PC projections, we calculate feature contributions for linear PCA (Fig. 4A) and plot the individual properties' distributions in the PC space for cosine Kernel-PCA (Fig. 4B-E). Due to the inherent non-linearity of Kernel-PCA, it is not possible to calculate feature contributions as for linear PCA.

Considering that "quiet and extreme" margins project at low PC1 values, Fig. 4 shows some general trends: "quiet and extreme" segments appear to have a combination of high sediment thickness, shallow dip angles, slow relative plate velocities, and low roughness, whereas "active and moderate" segments are characterised by a combination of lower sediment thickness, steeper dip angles, faster convergence, and varying roughness. Observations of links between the respective individual properties and seismicity which support this assessment include Heuret et al. (2012) and Scholl et al. (2015) for sediment thickness, van Rijsingen et al. (2018) for roughness, and Muldashev and Sobolev (2020) for both sediment thickness and dip angle. While additional properties may influence seismicity, we demonstrate here that our unsupervised approach, using this property set, provides valuable insights into margin seismicity.

Considering the (likely non-linear) connections between combinations of margin properties and seismic behaviour found in this work, we suggest that moving forward, the search for linear correlations between individual properties should be abandoned in favour of studying margins in terms of their PCA profiles.

A Table: Variance explained and feature contributions for linear PCA.

Linear PCA	Variance explained	Sediment thickness	Dip angle	Relative plate velocity	Roughness
PC1	47.8%	-0.505	0.584	0.317	0.551
PC2	25.2%	0.523	-0.138	0.828	0.149

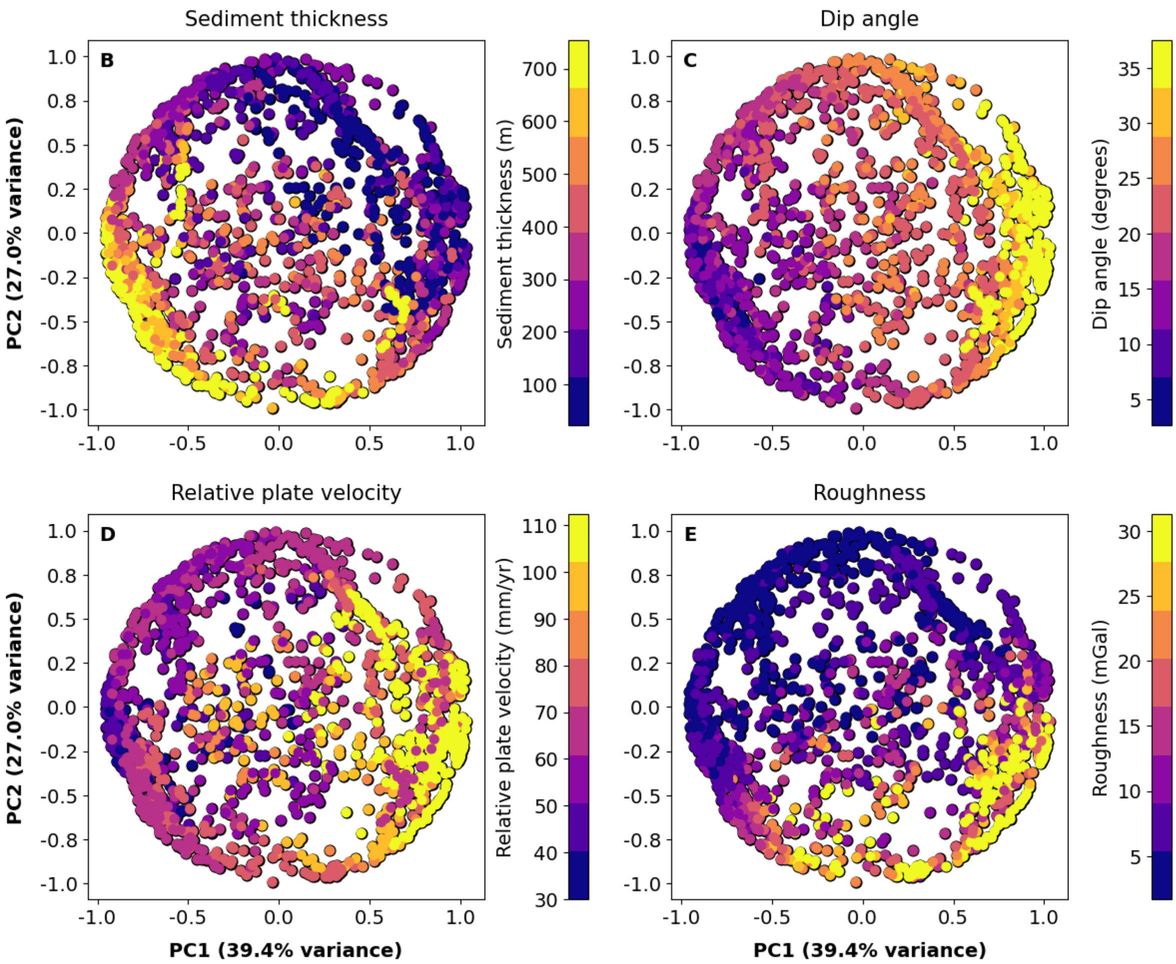

Figure 4: A. Table showing explained variance and feature importance for the linear PCA projections. **BCDE.** Property distributions in the PC space for cosine Kernel-PCA.

CONCLUSION

We explore the relationship between four margin properties – the subducting plate's dip angle, roughness, sediment thickness, and the plates' relative velocity – and maximum earthquake magnitudes using (Kernel-)PCA projections. This approach avoids bias from underestimated maximum magnitudes resulting from the short earthquake record.

We observe a distinct cluster of low-maximum magnitude segments in the PC space and suggest it represents “active and moderate” margins, contrasted by “low background seismicity, quiet and extreme” margins (as described by Ide, 2013). Using PCA projections to identify margins prone to giant earthquakes with no precedent in the instrumental record, we highlight the Hikurangi, Cascadia, Nankai-Ryukyu, Izu-Bonin, and Middle America margins.

Based on these (Kernel-) PCA projections, we suggest that seismic behaviour at subduction margins is describable as a non-linear combination of margin properties. We find that a combination of high sediment thickness, low dip angles, low roughness, and low relative plate velocity is generally associated with higher maximum magnitudes, while the opposite is generally true for lower maximum magnitudes. We argue that moving away from searching for linear connections between individual properties and towards studying margins in terms of their PCA profile opens up new pathways for understanding subduction margin seismicity.

ACKNOWLEDGEMENTS

This work is part of Valerie Locher’s MSc and PhD studies at Imperial College London, funded by the Department of Earth Science and Engineering’s computational science and engineering scholarship for women. The code utilizes the Python library scikit-learn. The authors thank Xiaodong Yang, Alex Whittaker, Saskia Goes, and three anonymous reviewers for their valuable feedback.

REFERENCES

Albini, P., Musson, R., Gomez Capera, A., Locati, M., Rovida, A., Stucchi, M., & Viganò, D. (2013). Global historical earthquake archive and catalogue (1000-1903). *Pavia, Italy*.

Bassett, D., & Watts, A. B. (2015). Gravity anomalies, crustal structure, and seismicity at subduction zones: 1. Seafloor roughness and subducting relief. *Geochemistry, Geophysics, Geosystems*, *16*(5), 1508-1540.

Brizzi, S., Sandri, L., Funiciello, F., Corbi, F., Piromallo, C., & Heuret, A. (2018). Multivariate statistical analysis to investigate the subduction zone parameters favoring the occurrence of giant megathrust earthquakes. *Tectonophysics*, *728*, 92-103.

Clark, K., Howarth, J., Litchfield, N., Cochran, U., Turnbull, J., Dowling, L., Howell, A., Berryman, K., & Wolfe, F. (2019). Geological evidence for past large earthquakes and tsunamis along the Hikurangi subduction margin, New Zealand. *Marine Geology*, *412*, 139-172.

Douglas, A., Beavan, J., Wallace, L., & Townend, J. (2005). Slow slip on the northern Hikurangi subduction interface, New Zealand. *Geophysical Research Letters*, *32*(16).

Fujiwara, O., Goto, K., Ando, R., & Garrett, E. (2020). Paleotsunami research along the Nankai Trough and Ryukyu Trench subduction zones–current achievements and future challenges. *Earth-Science Reviews*, *210*, 103333.

Heuret, A., Conrad, C., Funiciello, F., Lallemand, S., & Sandri, L. (2012). Relation between subduction megathrust earthquakes, trench sediment thickness and upper plate strain. *Geophysical Research Letters*, *39*(5).

Hubert, L., & Arabie, P. (1985). Comparing partitions. *Journal of classification*, *2*, 193-218.

Ide, S. (2013). The proportionality between relative plate velocity and seismicity in subduction zones. *Nature Geoscience*, *6*(9), 780-784.

Jolliffe, I. T. (2002). *Principal component analysis for special types of data*. Springer.

Lallemand, S., Peyret, M., van Rijsingen, E., Arcay, D., & Heuret, A. (2018). Roughness characteristics of oceanic seafloor prior to subduction in relation to the seismogenic potential of subduction zones. *Geochemistry, Geophysics, Geosystems*, *19*(7), 2121-2146.

Liu, Q., Lu, H., & Ma, S. (2004). Improving kernel Fisher discriminant analysis for face recognition. *IEEE transactions on circuits and systems for video technology*, *14*(1), 42-49.

McCaffrey, R. (2008). Global frequency of magnitude 9 earthquakes. *Geology*, *36*(3), 263-266.

McCaffrey, R. (2009). The tectonic framework of the Sumatran subduction zone. *Annual Review of Earth and Planetary Sciences*, *37*, 345-366.

McLellan, M., & Audet, P. (2020). Uncovering the physical controls of deep subduction zone slow slip using supervised classification of subducting plate features. *Geophysical Journal International*, *223*(1), 94-110.

Muldashev, I. A., & Sobolev, S. V. (2020). What controls maximum magnitudes of giant subduction earthquakes? *Geochemistry, Geophysics, Geosystems*, *21*(9), e2020GC009145.

Nakao, A., Kuwatani, T., Ueki, K., Yoshida, K., Yutani, T., Hino, H., & Akaho, S. (2023). Regression analysis and variable selection to determine the key subduction-zone parameters that determine the maximum earthquake magnitude. *Earth, Planets and Space*, *75*(1), 1-12.

Nishikawa, T., & Ide, S. (2015). Background seismicity rate at subduction zones linked to slab-bending-related hydration. *Geophysical Research Letters*, *42*(17), 7081-7089.

Nishimura, T., Matsuzawa, T., & Obara, K. (2013). Detection of short-term slow slip events along the Nankai Trough, southwest Japan, using GNSS data. *Journal of Geophysical Research: Solid Earth*, *118*(6), 3112-3125.

Rogers, G., & Dragert, H. (2003). Episodic tremor and slip on the Cascadia subduction zone: The chatter of silent slip. *Science*, *300*(5627), 1942-1943.

Ruff, L., & Kanamori, H. (1980). Seismicity and the subduction process. *Physics of the Earth and Planetary interiors*, *23*(3), 240-252.

Ruff, L. J. (1989). Do trench sediments affect great earthquake occurrence in subduction zones? *Subduction Zones Part II*, 263-282.

Satake, K., Shimazaki, K., Tsuji, Y., & Ueda, K. (1996). Time and size of a giant earthquake in Cascadia inferred from Japanese tsunami records of January 1700. *Nature*, *379*(6562), 246-249.

Schellart, W. P., & Rawlinson, N. (2013). Global correlations between maximum magnitudes of subduction zone interface thrust earthquakes and physical parameters of subduction zones. *Physics of the Earth and Planetary Interiors*, *225*, 41-67.

Schölkopf, B., Smola, A., & Müller, K.-R. (1998). Nonlinear component analysis as a kernel eigenvalue problem. *Neural computation*, *10*(5), 1299-1319.

Scholl, D. W., Kirby, S. H., von Huene, R., Ryan, H., Wells, R. E., & Geist, E. L. (2015). Great (≥ Mw8. 0) megathrust earthquakes and the subduction of excess sediment and bathymetrically smooth seafloor. *Geosphere*, *11*(2), 236-265.

Smith, M. W. (2014). Roughness in the earth sciences. *Earth-Science Reviews*, *136*, 202-225.

Stein, S., & Okal, E. A. (2007). Ultralong period seismic study of the December 2004 Indian Ocean earthquake and implications for regional tectonics and the subduction process. *Bulletin of the Seismological Society of America*, *97*(1A), S279-S295.

Stein, S., & Okal, E. A. (2011). The size of the 2011 Tohoku earthquake need not have been a surprise. *Eos, Transactions American Geophysical Union*, *92*(27), 227-228.

U.S. Geological Survey. (1900 - 2023). *Earthquake Catalog*. Retrieved August 09, 2023 from https://earthquake.usgs.gov/earthquakes/search/

van Rijsingen, E., Lallemand, S., Peyret, M., Arcay, D., Heuret, A., Funiciello, F., & Corbi, F. (2018). How subduction interface roughness influences the occurrence of large interplate earthquakes. *Geochemistry, Geophysics, Geosystems*, *19*(8), 2342-2370.

Wallace, L. M., Reyners, M., Cochran, U., Bannister, S., Barnes, P. M., Berryman, K., Downes, G., Eberhart-Phillips, D., Fagereng, A., & Ellis, S. (2009). Characterizing the seismogenic zone of a major plate boundary subduction thrust: Hikurangi Margin, New Zealand. *Geochemistry, Geophysics, Geosystems*, *10*(10).

Wasserstein, L. N. (1969). Markov processes on countable product space describing large systems of automata. *Probl. Pered. Inform*, *5*, 64-73.

Wells, D. L., & Coppersmith, K. J. (1994). New empirical relationships among magnitude, rupture length, rupture width, rupture area, and surface displacement. *Bulletin of the Seismological Society of America*, *84*(4), 974-1002.

Wirth, E. A., Sahakian, V. J., Wallace, L. M., & Melnick, D. (2022). The occurrence and hazards of great subduction zone earthquakes. *Nature Reviews Earth & Environment*, *3*(2), 125-140.

Supplemental Material

1. PCA and Kernel-PCA

Principal Component Analysis (PCA) (e.g. Jolliffe, 2002) is a method to project data into a different space, where the axes are the "Principal Components" (PCs), which represent the directions of the highest variance in a dataset. PCA calculates as many PCs as there are features (dimensions) in the original dataset and re-orients the data points into this new space. PCs are numbered in descending order of the proportion of variance of the original data distribution they capture, i.e. PC1 captures the most variance, PC2 the second most, etc.

In **Kernel-PCA** (Schölkopf et al., 1998), the data is projected into a higher-dimensional space using a kernel function before finding the PCs and reorienting the data points into the new space. This can allow for linear separation between clusters which are inseparable in the original space. For instance, considering two-dimensional data points, we can apply a function to add a third dimension: a point (x, y) will be transformed to (x, y, z) where $z = \phi(x, y)$ is calculated as a function ϕ of the original data (x, y). Using non-linear functions for ϕ, such as Gaussian, polynomial, or trigonometric functions, we can introduce non-linearity when transforming the data into the higher-dimensional space. Therefore, once the transformed, higher-dimensional data is projected into the PC space, the orientation of the PCs and data distribution may capture non-linear patterns in the original data. Fig. S1 shows a conceptual illustration of these steps.

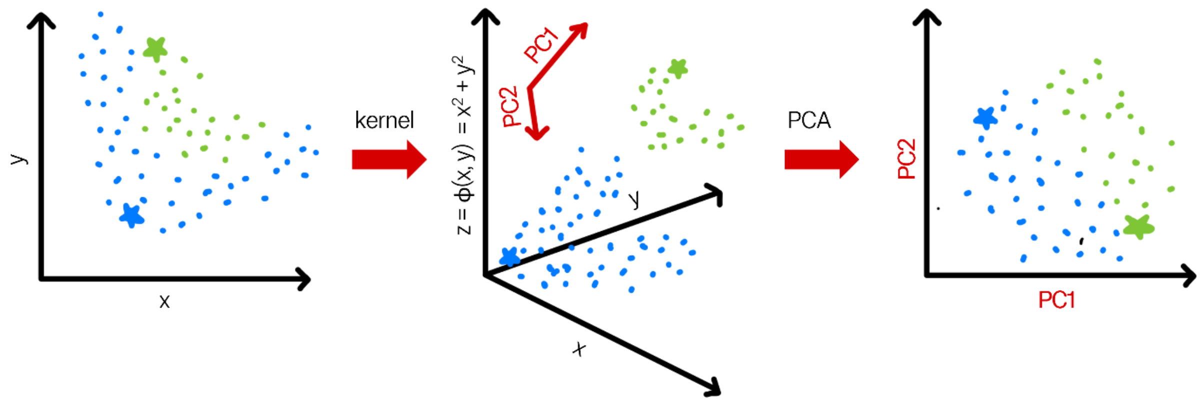

Fig. S1: Sketch illustrating the steps of Kernel-PCA. Here, the new dimension z is calculated as $\phi(x, y) = x^2 + y^2$.

However, transforming large, high-dimensionality datasets into even higher-dimensional spaces is computationally expensive. Instead, the "kernel trick" is used to avoid having to transform each data point by instead calculating the similarity between each combination of two data points. Kernels are functions that measure the similarity between two points x and y (described as vectors), for example:

- **Radial Basis Function (RBF) kernel (Gaussian):** $k(x, y) = \exp\left(\frac{||x-y||^2}{2\sigma^2}\right)$ where σ is a free parameter defining the width of the Gaussian curve; in scikit-learn, it is expressed as γ where $\gamma = \frac{1}{2\sigma^2}$
- **Cosine kernel** (Liu et al., 2004): $k'(x, y) = \frac{k(x,y)}{\sqrt{k(x,x)k(y,y)}}$ where k is a polynomial kernel
- **Polynomial kernel:** $k(x, y) = (x \cdot y)^d$ where d is the degree of the polynomial

The difference between these kernels is that they use different methods to calculate the similarity between two points. For instance, the RBF kernel calculates the similarity as the likelihood of a point x belonging to a Gaussian curve centered around another point y. Applying a cosine kernel is comparable to calculating the cosine of the angle between the two points' vectors (Liu et al., 2004). Thus, for the cosine kernel's calculation of similarity, the direction in which points lie is more important than the Euclidean distance between them.

In conclusion, Kernel-PCA allows us to look for non-linear patterns in datasets, and that different kernels result in different PCA projections owing to the similarity calculation used.

2. Data Scaling

Scaling or standardizing data prior to PCA is critical. We use scikit-learn's built-in scaler functions, which are defined as:

- StandardScaler: $x_{scaled} = \frac{x - mean}{standard\ deviation}$
- RobustScaler: $x_{scaled} = \frac{x - median}{interquantile\ range}$ where the interquantile range describes the difference between the 25th and 75th quantiles
- MinMaxScaler: $x_{scaled} = \frac{x - minimum}{maximum - minimum}$, where the maximum and minimum are the largest and smallest feature values

For more information, see the documentation of scikit-learn scalers.

3. Supplemental figures and tables

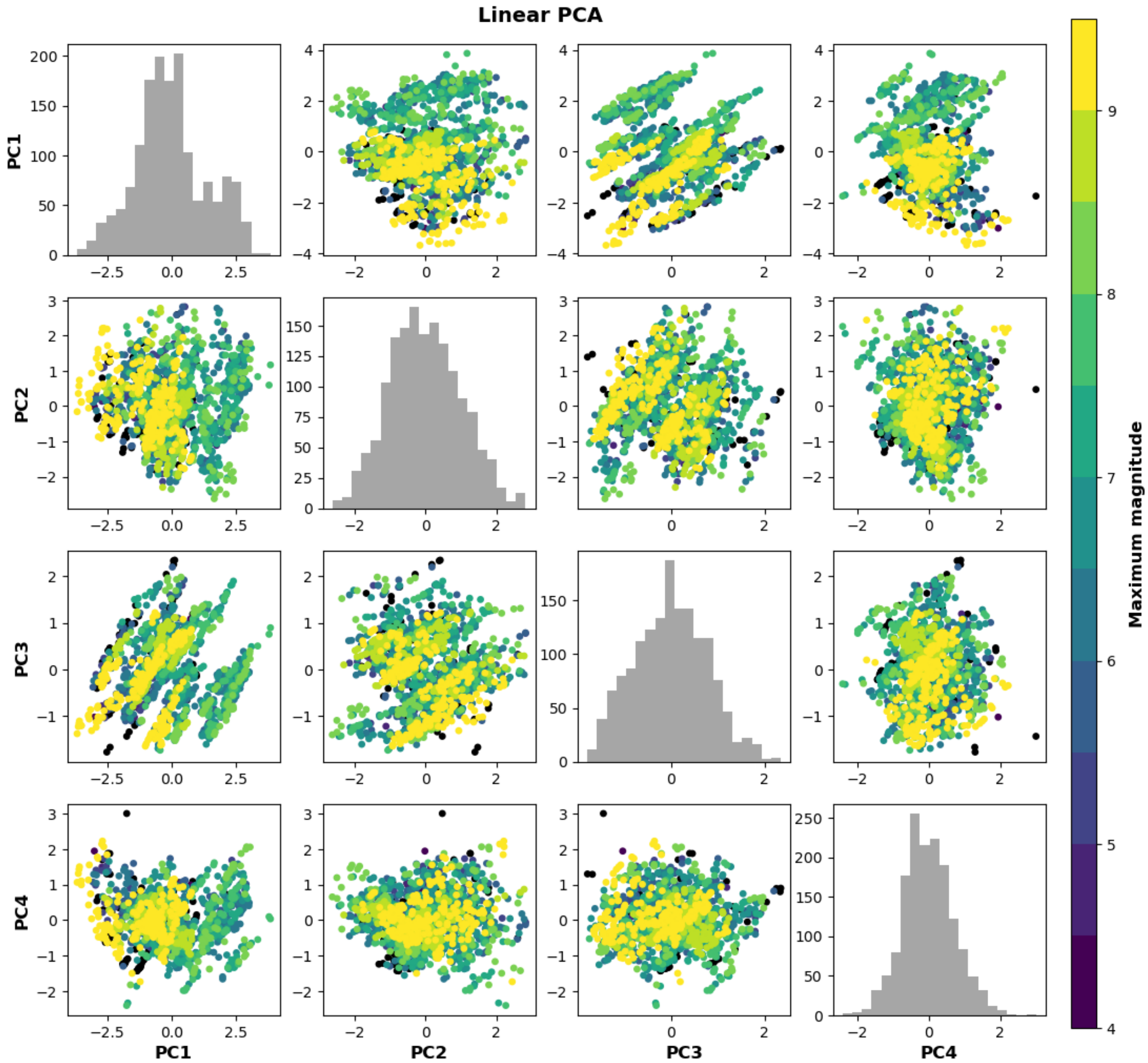

Fig. S2: Full pair plots for linear PCA, colour coded by maximum magnitude.

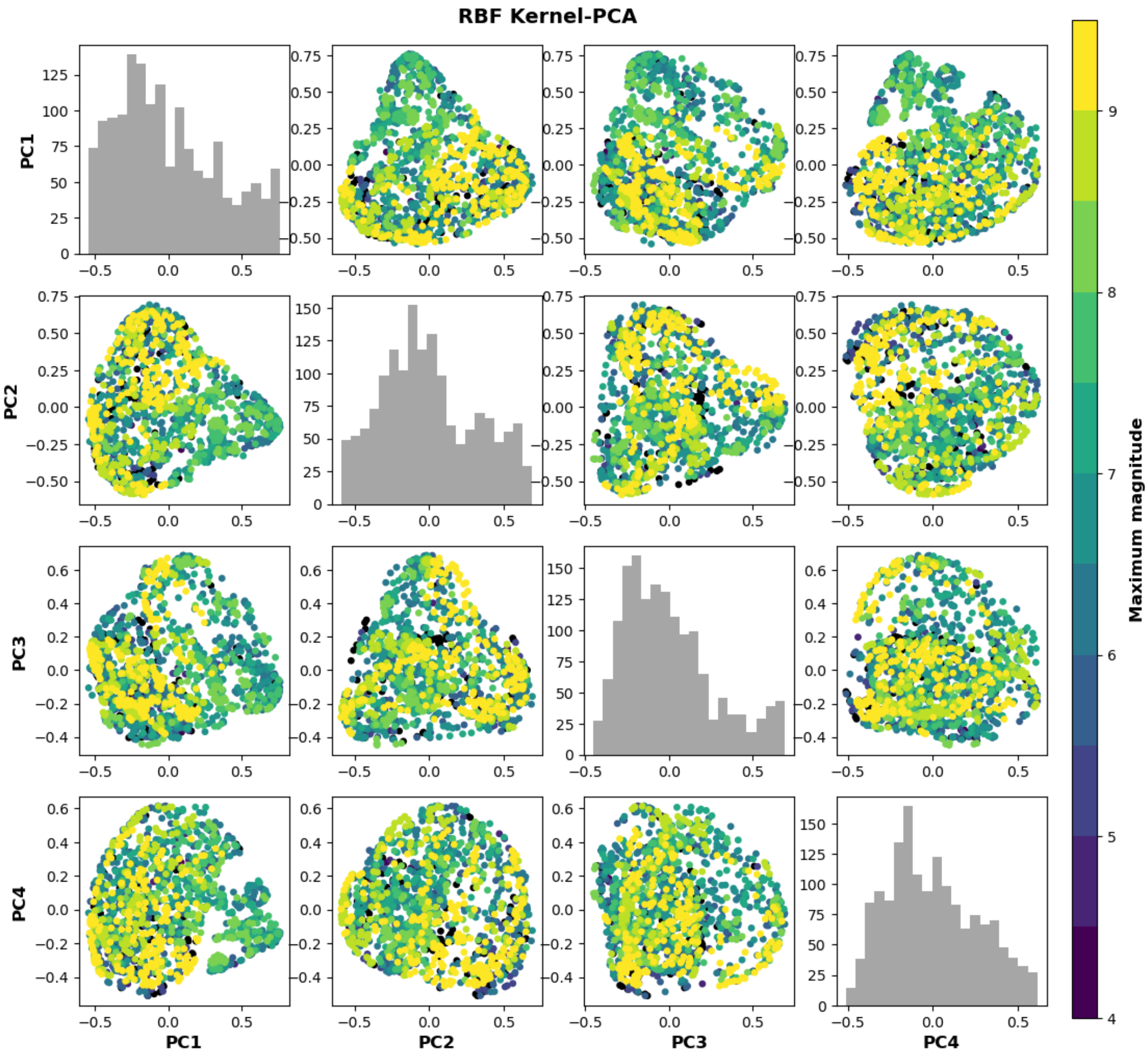

Fig. S3: Pair plots of PC1 through PC4 for RBF Kernel-PCA, colour coded by maximum magnitude.

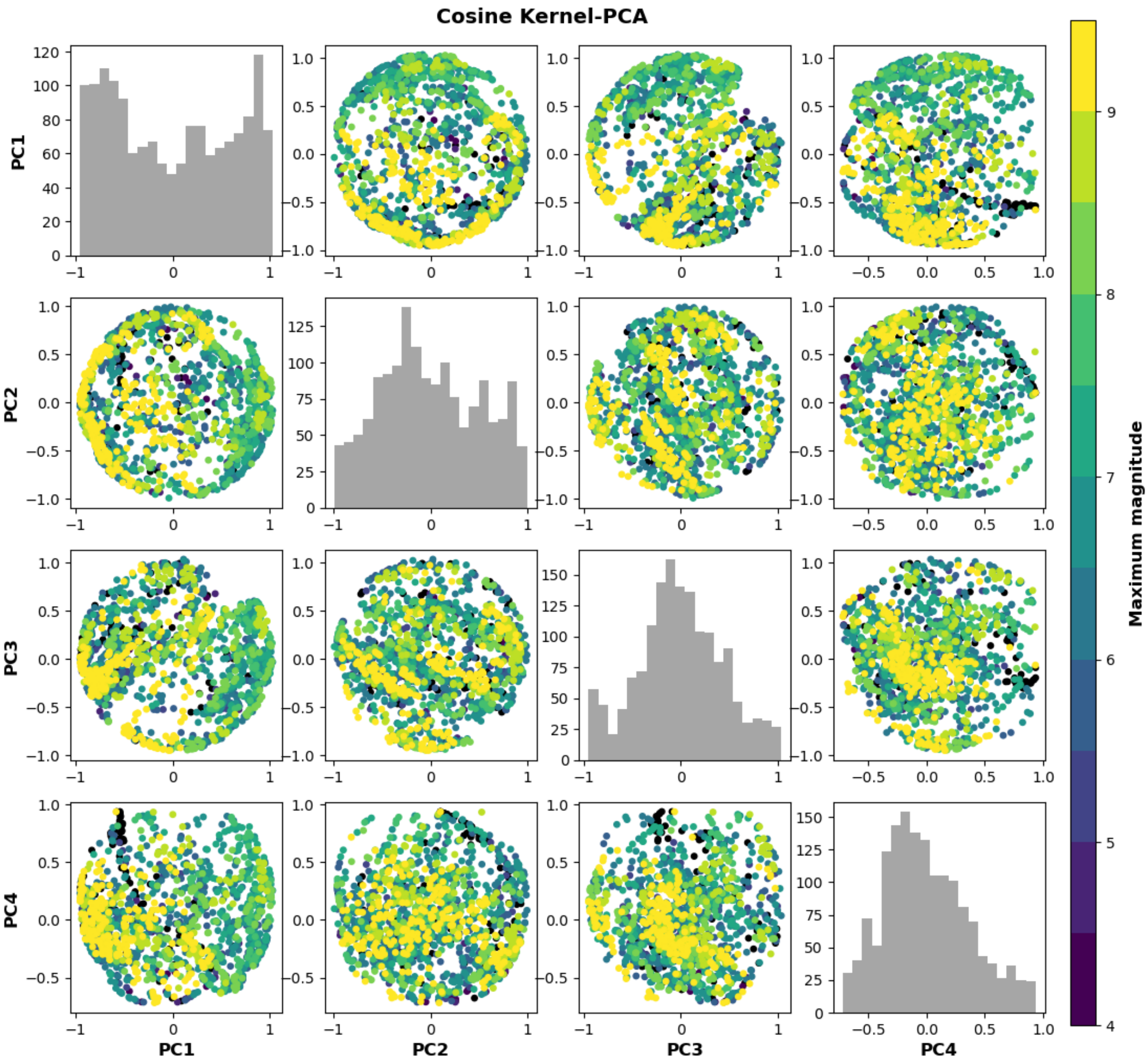

Fig. S4: Full pair plots for cosine Kernel-PCA, colour coded by maximum magnitude.

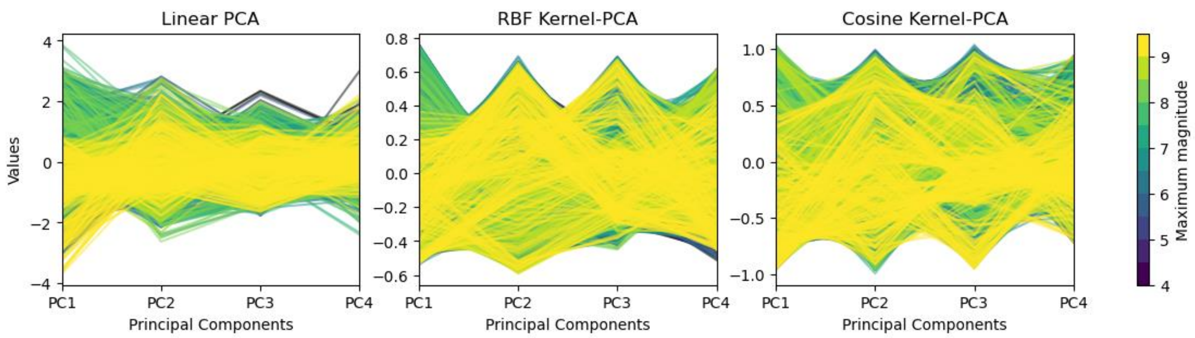

Fig. S5: Parallel coordinates plot for PC1 through PC4 for linear, RBF Kernel- and cosine Kernel-PCA.

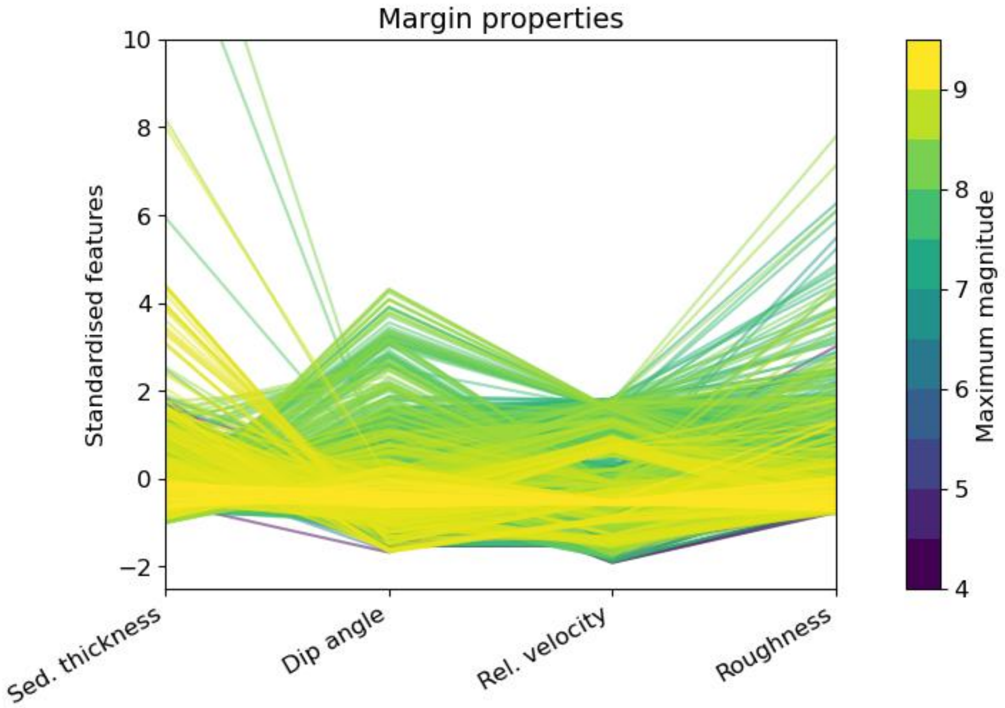

Fig. S6: Parallel coordinates plot the original (standardized) margin properties.

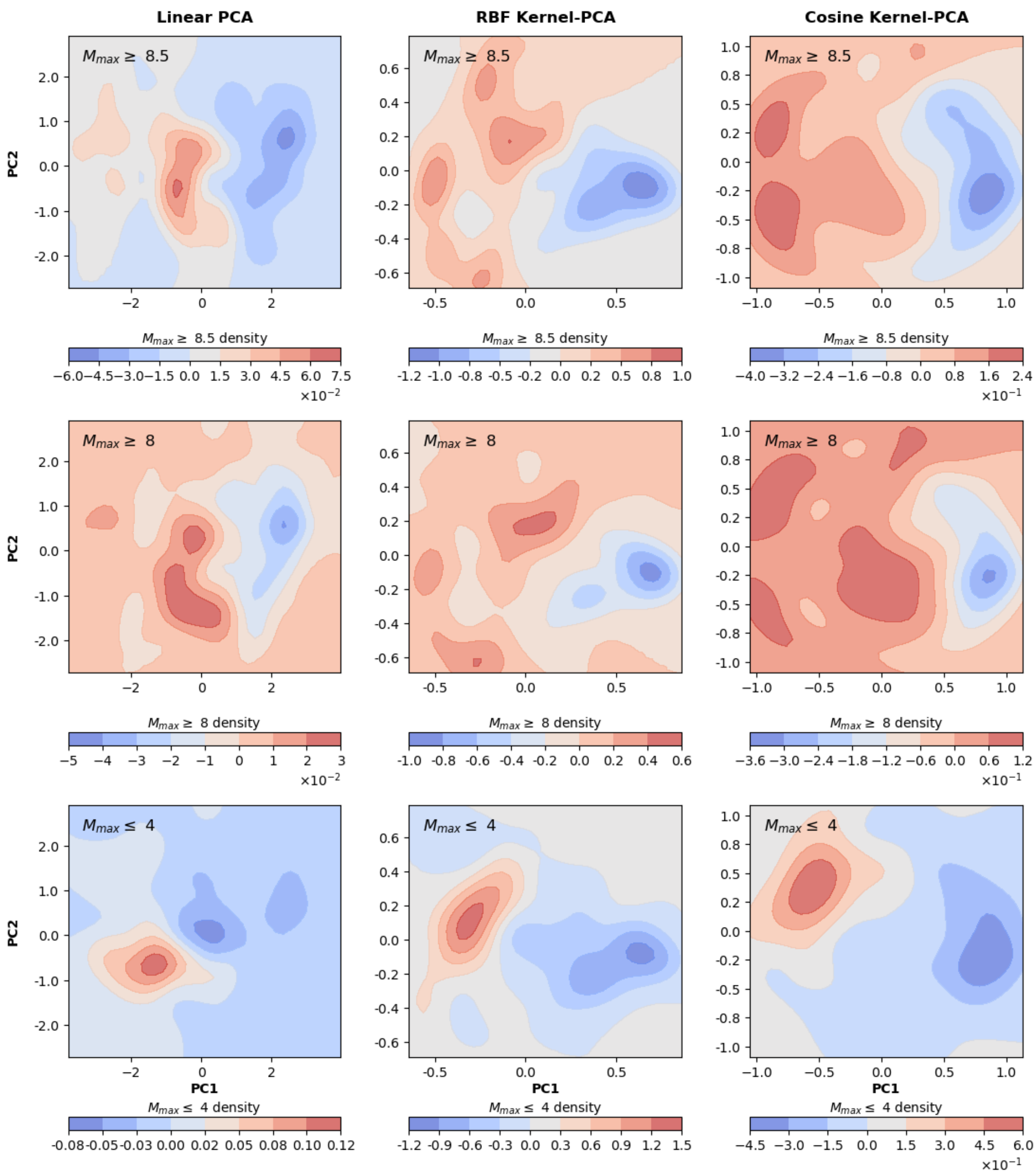

Fig. S7: Density difference maps for different magnitude cutoffs (≥ 8.5, ≥8, and ≤4) for linear PCA, RBF and Cosine Kernel-PCA. This illustrates a) that changing the magnitude threshold from 8.5 to 8 results in the same pattern, demonstrating our method is robust to this change, and b) that segments of maximum magnitude ≤ 4 (“quiet”) project in the same area as segments of high (≥ 8.5 or ≥8) maximum magnitude (“extreme”).

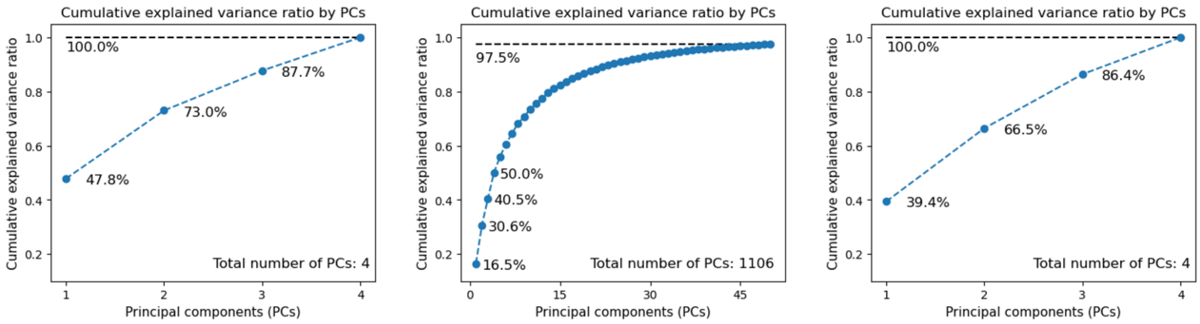

408

409 **Fig. S8:** Cumulative variance explained from linear PCA, RBF and cosine Kernel-PCA.

410

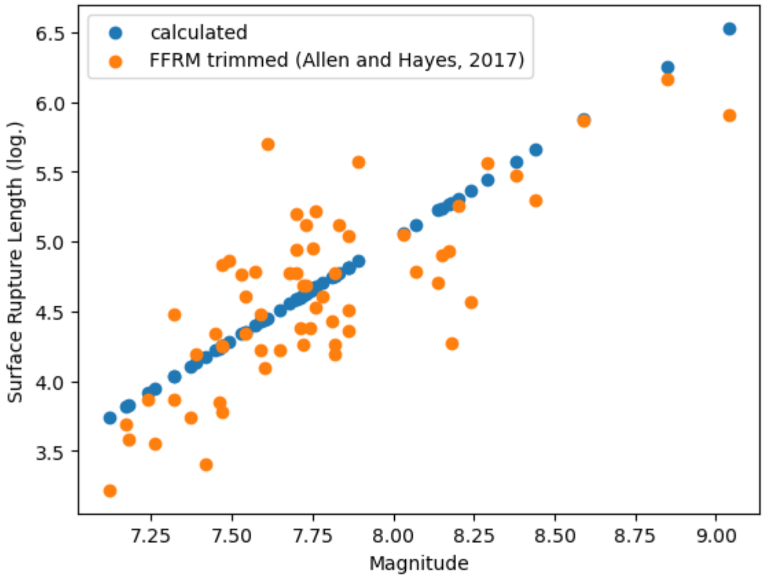

411

412 **Fig. S9:** Surface rupture lengths (logarithmic scale) as estimated from earthquake magnitudes (Wells
413 & Coppersmith, 1994) in our approach, compared to their corresponding finite fault rupture models
414 (using data compiled by Allen & Hayes, 2017). This shows the Wells and Coppersmith estimates are a
415 reasonable estimate for surface rupture length, validating our method.

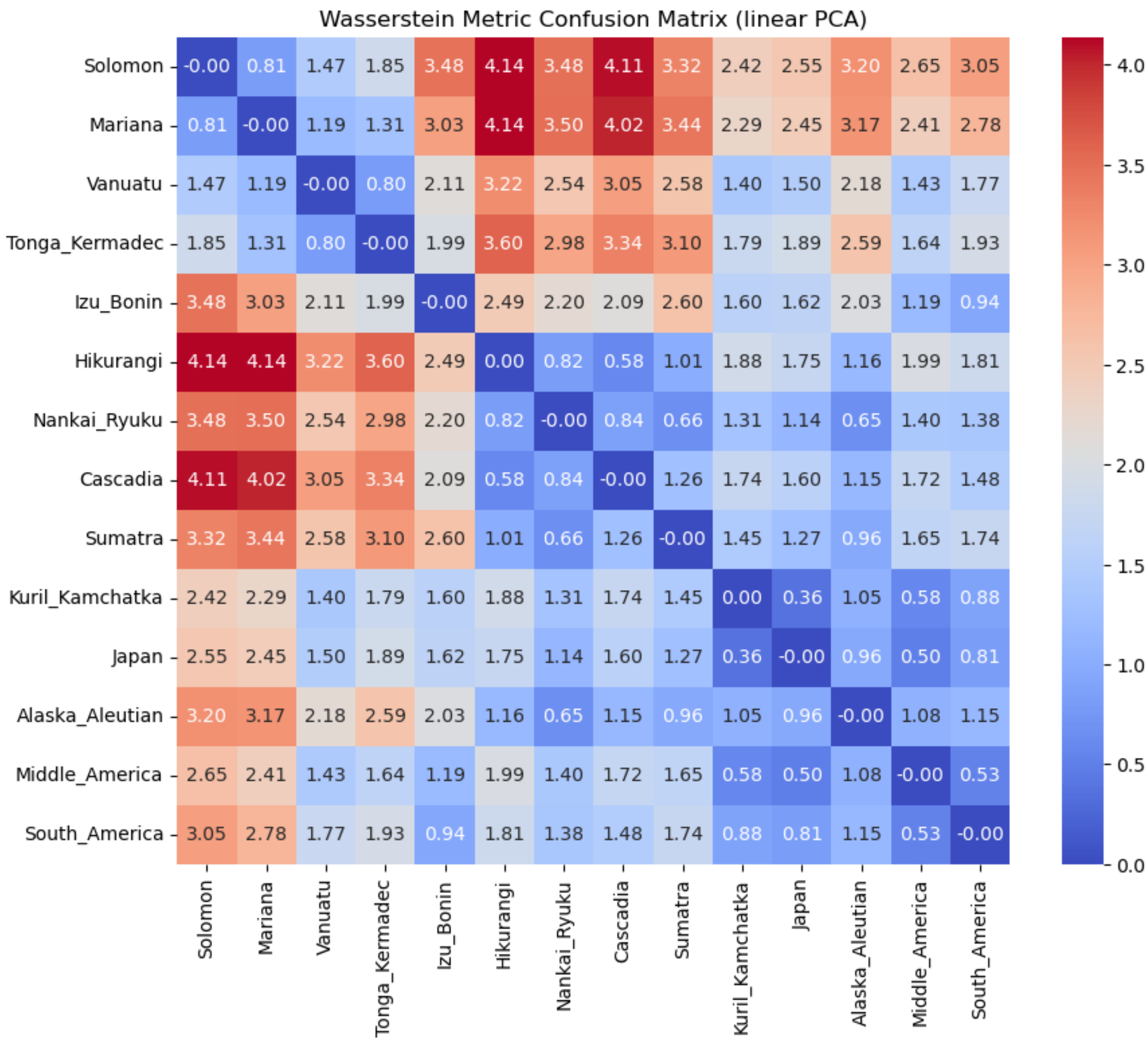

Fig. S10: Wasserstein distances calculated for margin clusters in the linear PCA projection. Low Wasserstein distances indicate that the PC space clusters of the two margins are close, reflecting similar PCA profiles and margin properties. In contrast, high Wasserstein distances suggest the clusters are far apart, indicating the two margins have distinct PCA profiles and property combinations.

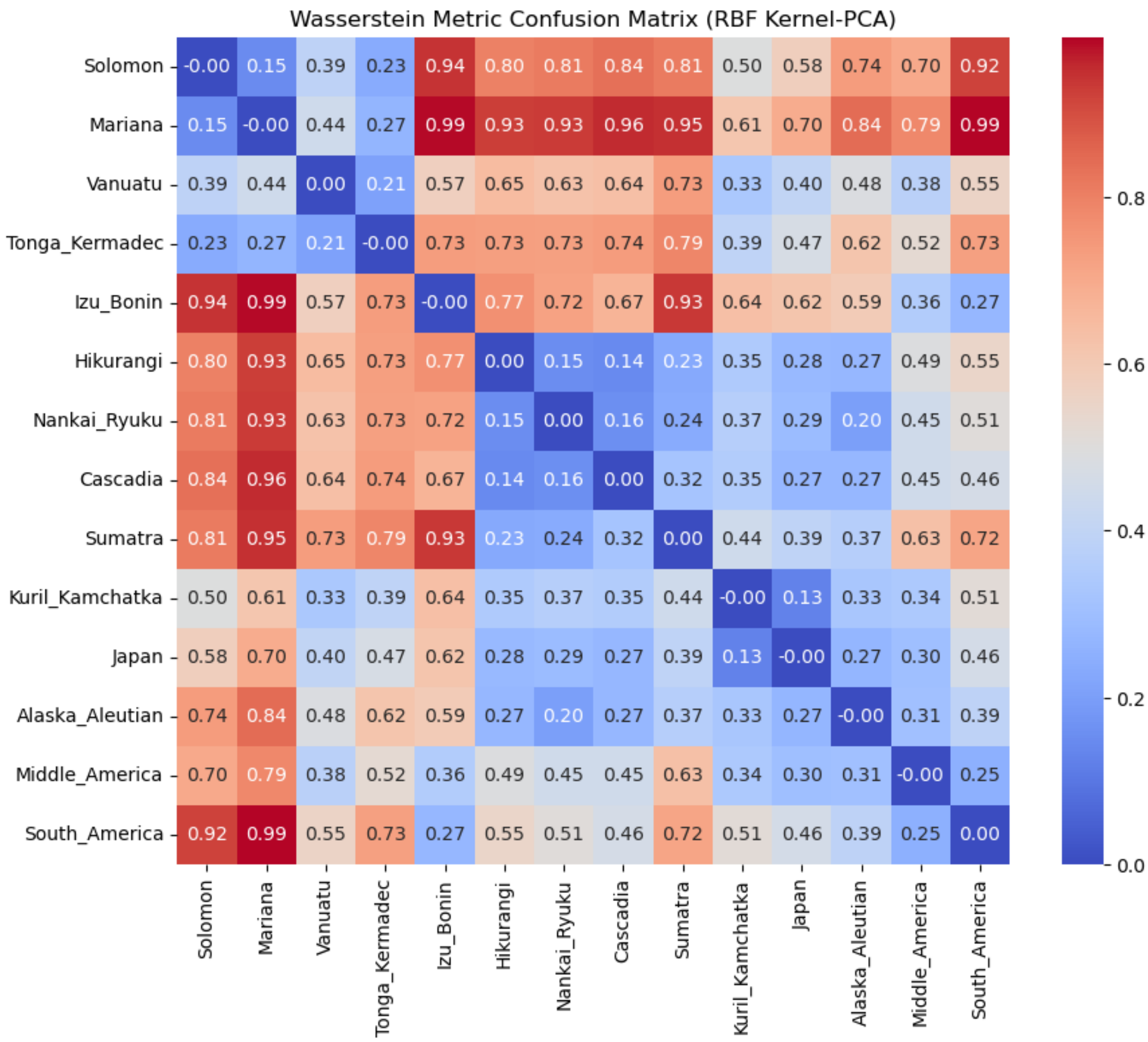

Fig. S11: Wasserstein distances calculated for margin clusters in the RBF Kernel-PCA projection. Low Wasserstein distances indicate that the PC space clusters of the two margins are close, reflecting similar PCA profiles and margin properties. In contrast, high Wasserstein distances suggest the clusters are far apart, indicating the two margins have distinct PCA profiles and property combinations.

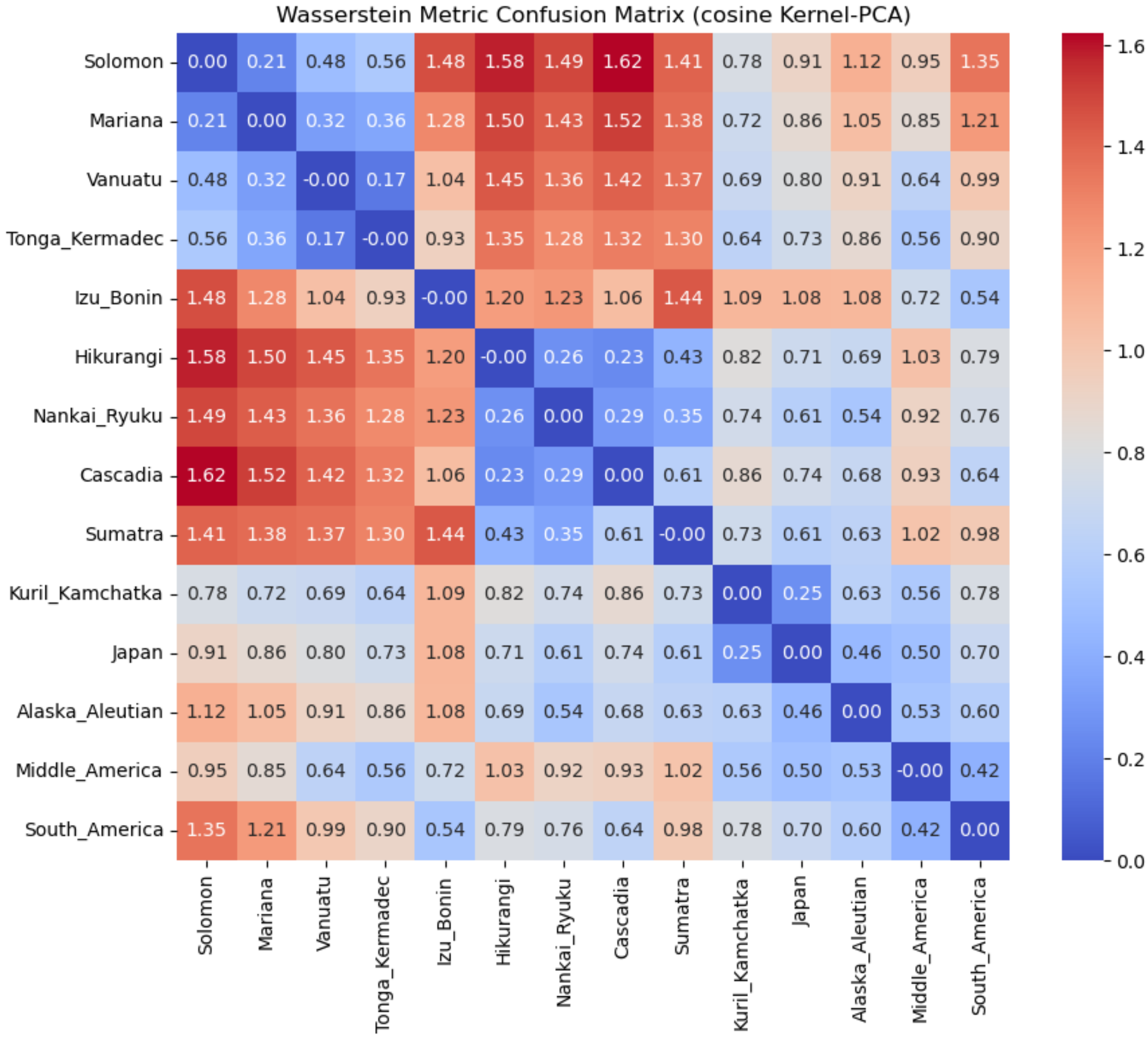

Fig. S12: Wasserstein distances calculated for margin clusters in the cosine Kernel-PCA projection. Low Wasserstein distances indicate that the PC space clusters of the two margins are close, reflecting similar PCA profiles and margin properties. In contrast, high Wasserstein distances suggest the clusters are far apart, indicating the two margins have distinct PCA profiles and property combinations.

References

Allen, T. I., & Hayes, G. P. (2017). Alternative rupture-scaling relationships for subduction interface and other offshore environments. *Bulletin of the Seismological Society of America*, *107*(3), 1240-1253.

Jolliffe, I. T. (2002). *Principal component analysis for special types of data*. Springer.

Liu, Q., Lu, H., & Ma, S. (2004). Improving kernel Fisher discriminant analysis for face recognition. *IEEE transactions on circuits and systems for video technology*, *14*(1), 42-49.

Schölkopf, B., Smola, A., & Müller, K.-R. (1998). Nonlinear component analysis as a kernel eigenvalue problem. *Neural computation*, *10*(5), 1299-1319.

Wells, D. L., & Coppersmith, K. J. (1994). New empirical relationships among magnitude, rupture length, rupture width, rupture area, and surface displacement. *Bulletin of the Seismological Society of America*, *84*(4), 974-1002.